THE JOURNAL OF BIOLOGICAL CHEMISTRY VOL. 287, NO. 15, pp. 12204–12216, April 6, 2012

Cell Surface Proteoglycans Syndecan-1 and -4 Bind Overlapping but Distinct Sites in Laminin α3 LG45 Protein Domain*

Received for publication, September 1, 2011, and in revised form, January 25, 2012 Published, JBC Papers in Press, February 20, 2012, DOI 10.1074/jbc.M111.300061

Sonia Carulli[‡1], **Konrad Beck**[§], **Guila Dayan**[‡], **Sophie Boulesteix**[‡], **Hugues Lortat-Jacob**[¶], **and Patricia Rousselle**[‡2]

From the [‡]*Structure Fédérative de Recherche BioSciences Gerland-Lyon Sud, Institut de Biologie et Chimie des Protéines, FRE 3310, CNRS, Université Lyon 1, 7 Passage du Vercors, 69367 Lyon, France, the* [§]*Cardiff University School of Dentistry, Heath Park, Cardiff CF14 4XY, United Kingdom, and the* [¶]*Commissariat à l'Energie Atomique, CNRS, Université Joseph Fourier-Grenoble 1, Institut de Biologie Structurale Jean-Pierre Ebel, UMR 5075, 38000 Grenoble, France*

Background: The cell surface proteoglycans syndecan-1 and -4 interact with laminin 332 to participate in keratinocyte migration.
Results: Syndecan-1 and -4 bind specific residues in the laminin 332 LG45 domain.
Conclusion: The LG45 domain encompasses a major heparan sulfate binding domain containing distinctive syndecan-1 and -4 binding sequences.
Significance: Identifying syndecan-1- and -4-binding sites in laminin 332 is crucial for elucidation of their function in keratinocyte migration.

Keratinocyte migration during epidermal repair depends on interactions between cellular heparan sulfate proteoglycan receptors, syndecan-1 and -4, and the C-terminal globular domains (LG45) of the extracellular matrix protein laminin 332. This study investigates the molecular basis of the binding specificity of the syndecan-1 and -4 receptors expressed by human keratinocytes. We used site-directed mutagenesis to alter a recombinant LG45 protein by substituting the most critical basic residues with glutamine. All proteins were expressed in mammalian cells, purified, and characterized biochemically. We used *in vitro* binding assays, including surface plasmon resonance, to examine interactions between mutated LG45 and heparan sulfates, syndecan-1 and -4. We identify a major heparin binding domain on the outer edge of a β-strand of LG45 surrounded by a track of converging low affinity residues. This domain harbors distinctive syndecan-1 and -4 binding-specific sequences. This is the first study to demonstrate a binding specificity of two proteoglycans produced by a single cell type. In addition, we found that although syndecan-1 interacts exclusively through its glycosaminoglycan chains, syndecan-4 binding relies on both its core protein and its heparan sulfate chains. These results suggest that LG45 may trigger different signals toward keratinocytes depending on its interaction with syndecan-1 or -4.

Cell adhesion to the extracellular matrix (ECM)[3] stimulates signal transduction cascades that are known to play critical regulatory roles in many biological processes, including wound healing (1–3). Although integrins are the major cell surface receptors for the ECM, transmembrane proteoglycans, such as syndecans, compose an important class of adhesion receptors that have recently attracted attention. Syndecans consist of transmembrane core proteins that carry either heparan sulfate (HS) or HS and chondroitin sulfate (CS) chains on their ectodomain. Through these chains, syndecans interact with growth factors, cytokines, proteinases, other adhesion receptors and ECM components. There are four syndecans in mammals, which are expressed in a developmental cell type- and tissue-specific manner (4, 5). Among numerous ligands within the ECM, recent studies have shown that laminins (LNs) can interact with these heparan sulfate proteoglycan (HSPG) receptors to fulfill important cellular events (6).

LNs are large extracellular glycoproteins that are important components of all basement membranes (BM), and they are involved in several biological processes (7). All LNs are cross-shaped heterotrimers composed of three different gene products, termed α, β, and γ chains. Over 16 LN isoforms are known with variable cell- and tissue-specific expression, and they are differentially recognized by cellular receptors (8). Laminin 332 (LN332), composed of the α3, β3, and γ2 chains, is an epithelial BM-specific variant. Its main role in normal tissues is the maintenance of epithelial-mesenchymal cohesion in tissues exposed to external forces, including skin and stratified squamous mucosa (9, 10). All LN α chains possess a large globular domain at the C-terminal end that consists of five homologous sub-

* This work was supported in part by Agence Nationale de la Recherche Grants ANR-08-PCVI-0031 and ANR-09-EBIO-023, Association pour la Recherche sur le Cancer Grant 1128, and Ligue Nationale Contre le Cancer.
[1] Recipient of a Ph.D. studentship from the Rhône-Alpes region (Program Cible) and from the Fondation pour la Recherche Médicale.
[2] To whom correspondence should be addressed: Institut de Biologie et Chimie des Protéines, 7 Passage du Vercors, 69367 Lyon Cedex 07, France. Tel.: 33-4-72-72-26-39; Fax: 33-4-72-72-26-02; E-mail: patricia.rousselle@ibcp.fr.

[3] The abbreviations used are: ECM, extracellular matrix; LN, laminin; LN332, laminin 332; HSPG, heparan sulfate proteoglycan; GAG, glycosaminoglycan; HS, heparan sulfate; CS, chondroitin sulfate; HBD, heparin binding domain; Ni-NTA, nickel-nitrilotriacetic acid; BM, basement membrane; NHK, normal human keratinocyte; SPR, surface plasmon resonance.

domains, each containing about 200 residues (LG1–5) (11). A potential function for the tandem LG4-LG5 domains (LG45) was initially suspected based on the ability of LN332 to trigger distinct cellular events depending on the level of processing of its α3 chain. A form of LN332 that lacked the LG45 was found in mature BMs, where it was shown to play an important function in the maintenance of anchoring structures through integrin interactions (12–14). In contrast, LN332 with an intact LG45 was found in migratory/remodeling situations such as epidermal repair (15–18). Recently, full-length LN332 (with LG45) was proposed to be involved in the invasion of squamous cell carcinomas *in vivo* (19).

The mechanism underlying the function of the LG45 domain in LN332 remains poorly understood. Several heparin binding domains (HBD) were identified in the LG45 domain of the α3 chain (α3LG45). These HBDs conferred heparin-dependent cell adhesion properties, which suggested that this region in LN332 could interact with an HSPG cellular receptor (20–22). Later, a motif in the LG45 domain that included residues ^{1412}NSFMALYLSKGR was shown to induce syndecan-2- and -4-mediated cell adhesion, neurite outgrowth, and matrix metalloproteinase-1 and -9 secretion (23–26). Further work suggested that this peptide motif also induced keratinocyte migration by triggering syndecan-4 clustering and subsequent β1 integrin activation (27). Others have reported that syndecan-1 was the cellular receptor involved in cell adhesion to the α3LG45 domain through its HS and CS chains (28, 29). This interaction could drive keratinocyte migration by inducing the formation of actin-based cellular protrusions and recruiting syntenin-1 (30, 31). The first heparin/syndecan-binding sites on LN332 were identified by peptide screening; however, a more recent study identified three novel HBDs based on cross-linking the native protein to heparin beads (22).

We wondered whether syndecan-1 and -4 interacted with a unique or multiple sequences in the LN332 LG45 domain. To address this question, we aimed to identify residues involved in the interaction between cells and the α3LG45 domain and to determine the molecular basis of the syndecan-1 and -4 interaction. By site-directed mutagenesis, we have identified the syndecan-1- and -4-binding sites in the α3LG45 domain and have demonstrated that these domains belong to a unique HBD. We further showed that these two receptors bound specifically to overlapping but independent sites through different mechanisms, in addition to the GAGs chains, as the core protein participates in syndecan-4 binding.

EXPERIMENTAL PROCEDURES

Cells and Antibodies—Fibrosarcoma HT1080 cells (CCL-212, American Type Culture Collection) were cultured in Dulbecco's modified Eagle's medium (DMEM) containing 2 mM glutamine and 10% fetal calf serum. Normal human keratinocytes (NHK) cultures were established from foreskin in KBM-2 medium (Cambrex Bio-Sciences, Emerainville, Belgium) as described previously (9). The human keratinocyte cell line HaCat was grown in 50% Ham's F-12 and 50% DMEM supplemented with 2 mM glutamine and 10% fetal calf serum. The polyclonal antibody (pAb) against syndecan-1 was obtained by rabbit immunization with the GST-syn-1 fusion protein (31); the rabbit pAb H-174 against syndecan-1 was purchased from Santa Cruz Biotechnology (Le Perray en Yvelines, France); the rabbit pAb S9111-60 against syndecan-4 was purchased from US Biologicals (distributed by Euromedex, Mundolsheim, France), and the anti-HS F58-10E4 was from Seikagaku (distributed by AMS Biotechnology, Oxfordshire, UK). The pAb against the LG45 fragment was described elsewhere (29).

Plasmids and Transfection—The human laminin α3LG45 domain (nucleotides 4057–5142) was generated by RT-PCR amplification of poly(A)$^+$ mRNA isolated from NHK with the following primers: 5′-GAATTCGAATTCGCTAGCTTGCTCACCACTTCCCAAGACCCAGGCC and 5′-TCTAGATCTAGATGCGGCCGCCTGGTCAGGACAACCATTCAGACTGAC. The resulting PCR product of 1080 bp was restriction-digested with NotI and NheI and inserted in-frame with sequences that encoded the BM-40 signal peptide and the six-histidine tag in the mammalian expression vector pCEP-Pu (32). Site-directed mutagenesis was performed on the LG45 sequence to substitute the lysine and arginine residues (single, double, or triple, as indicated in Fig. 1) to glutamine. This was accomplished by PCR amplification with oligonucleotides that contained the mutation sequences. The mutated PCR products were cloned into pCEP-Pu. All inserts and borders were fully sequenced (Genome Express, Meylan, France). These vectors were stably transfected into 293-EBNA cells (Invitrogen) with the FuGENE 6 reagent (Roche Diagnostics). Transfected cells were selected with 0.5 μg/ml puromycin and grown to confluence. Conditioned medium samples from transfected and wild type cells were analyzed with SDS-PAGE to confirm the secretion of WT and mutated recombinant LG45-His_6 fusion peptides into the medium.

Fusion proteins between GST and the human syndecan-1 and -4 ectodomains (GST-hS1ED and GST-hS4ED, respectively) were produced as followed. To append the ectodomain of syndecan-1 (Gln-18 to Gln-232) and syndecan-4 (Glu-19 to Phe-141) to the C terminus of GST, the cDNA encoding these domains was amplified by PCR, subcloned into EcoRI and NotI sites of pGEX-4T3 (GE Healthcare), and sequenced. GST fusion proteins were then produced in bacteria and purified on glutathione-Sepharose 4B beads (GE Healthcare) or 96-well glutathione-chelate plates (Nunc, Dutscher, Brumath, France) as recommended by the manufacturer's instructions.

Purification and Heparin Binding Assay for Recombinant LG45 Fragments—The recombinant LG45 proteins were secreted by transfected 293-EBNA cells cultured in serum-free DMEM. The conditioned medium was collected every 48 h, and 50 μM *N*-ethylmaleimide and 50 μM phenylmethanesulfonyl fluoride were added. To purify the His_6-tagged LG45 proteins, conditioned medium was mixed with imidazole (10 mM) and salt (0.3 M NaCl) and applied to 5-ml nickel/nitrilotriacetic acid columns (Ni-NTA Superflow Cartridge, Qiagen, Coutaboeuf, France). After washing with 50 mM NaH_2PO_4, 300 mM NaCl, 20 mM imidazole, proteins were eluted with a linear gradient of 20–400 mM imidazole. SDS-PAGE analysis showed an estimated protein purity of >90%. Protein concentration was determined with the bicinchoninic acid assay (Pierce). To evaluate protein affinity for heparin, LG45-His_6 proteins were placed in a 1-ml HiTrap heparin column (GE Healthcare) in

0.02 M Tris-HCl, pH 7.4, followed by elution with a linear gradient of 0–1 M NaCl. All the collected fractions were further analyzed by SDS-PAGE followed by Coomassie staining.

Cell Adhesion Assays—LG45 peptides were immobilized on multiwell nickel-chelate plates (Nunc). To ensure equal amounts and identical orientations of all immobilized proteins, multiwell plates were coated with serial dilutions of LG45 substrates in 0.01 M KCl and allowed to adsorb overnight at 4 °C. Plates were washed with PBS and saturated with 1% BSA. Next, HT1080 cells were prepared by detaching with 5 mM EDTA/PBS, followed by rinsing and suspending in serum-free medium; cells were seeded on LG45-coated plates at 8×10^4 cells/well. After 30 min, nonadherent cells were removed with a PBS wash. The extent of adhesion was determined by fixing adherent cells and then staining with 0.1% crystal violet and measuring absorbance at 570 nm as described previously (33). A blank value was subtracted that corresponded to BSA-coated wells. Each assay point was derived from triplicate measurements ± S.D. (three wells per assay point). Adherent cells were photographed with an Axiovert 40 Zeiss microscope coupled to a Coolsnap Fx Camera (Roper Scientific, Evry, France), and 100 cells (with or without protrusions) were counted in each well. The amount of adsorbed protein was determined with a BCA microprotein assay.

Time Lapse Video Microscopy—NHKs were seeded at 10^4 cells/well in 24-well plates in KBM-2 medium that contained either WT or mutated LG45-His_6 (20 μg/ml). Cell behavior was monitored at 37 °C for 24 h in a humidified atmosphere containing 5% CO_2 with an Axiovert 100 M Zeiss microscope equipped with a CCD camera (one picture every 20 min). In each experiment, we analyzed movements of 80–100 cells with tracking software (Metaview; Roper Scientific, Princeton Instruments, Evry, France). The maximal relative distances to origin (MRDO), defined as the linear distance between the original position of the cell and the farthest position of the cell (34), were determined.

Syndecan-1 and -4 Binding Assays—HaCat, NHK, or HT1080 cells were extracted with cold RIPA lysis buffer (20 mM Tris-HCl, pH 7.4, 150 mM NaCl, 2 mM EDTA, 250 μM phenylmethylsulfonyl fluoride, 1 mM *N*-ethylmaleimide, 1% Nonidet P-40, 1% Triton X-100, 0.1% sodium deoxycholate, 0.1% SDS). All the following procedures were performed at 4 °C. After centrifugation, lysate protein concentrations were determined, and equivalent amounts of proteins were tested in either ELISA-based syndecan-1 and -4 binding assays or affinity precipitation experiments. The ELISA-based assay was performed with 96-well nickel-chelate plates, coated with WT or mutated LG45-His_6, as described above. After plates were saturated with 1% BSA for 4 h at 4 °C, cell lysates were added (300 μg/well) and incubated overnight at 4 °C. After washes with lysis buffer and PBS, plates were incubated for 3 h with anti-syndecan-1 or anti-syndecan-4 pAbs. The plates were then washed with PBS and incubated with appropriate FITC-conjugated secondary antibodies (Jackson ImmunoResearch) for 1 h. After PBS washes, 50 μl of 20 mM NH_4OH with Triton 0.5% was added to each well, and fluorescence intensity was determined at 485–535 nm with a VICTOR X4 Technologies reader (PerkinElmer Life Sciences). A blank value corresponding to BSA-coated wells was systematically subtracted, and each assay point was derived from triplicate measurements. In case of pretreatment with heparitinase I, cells were incubated in digestion buffer (20 mM sodium acetate, pH 7.0, 5 mM $CaCl_2$) with or without 8 milliunits/ml heparitinase I (Seikagaku America, Coger, Paris, France) for 4 h at 25 °C prior to the lysis in RIPA buffer.

For syndecan-1 and -4 pulldown experiments, 100 μg of WT or mutated LG45-His_6 proteins were linked to nickel magnetic beads (Millipore SAS, Molsheim, France) for 2 h at 4 °C in incubation buffer (50 mM NaH_2PO_4, pH 8, 300 mM NaCl). Next, beads were washed in incubation buffer, followed by incubation with 1 mg of cell lysis extract, supplemented with 10 mM imidazole for 2 h. Beads were then washed in lysis buffer with 20 mM imidazole and incubated in digestion buffer with 8 milliunits/ml heparitinase I and 50 milliunits/ml chondroitinase ABC for 2 h at 25 °C. Proteins were resolved on 8 or 10% SDS-polyacrylamide gels. Separated proteins were transferred to nitrocellulose, followed by immunodetection of syndecan-1 or syndecan-4 by enhanced chemiluminescence.

GST-syndecan-1 and -4 ectodomains were immobilized on multiwell glutathione-chelate plates (Nunc). The wells were blocked with 4% milk in PBS and incubated with soluble LG45 (10 μg/ml) for 4 h at 22 °C. They were further exposed (1 h, 22 °C) to a constant amount of anti-LG45 pAb, and detection was performed using FITC-conjugated antibodies as described above.

Circular Dichroism (CD) Spectroscopy—CD spectra were recorded on an Aviv Model 215 instrument (Aviv Biomedical Inc., Lakewood, NJ; 1-nm bandwidth, 0.2-nm steps, 3–5 s per point accumulation time) equipped with a thermostatted cell holder. Buffer baselines were recorded in the same cell and subtracted. Data were smoothed and normalized to mean residue ellipticities $[\Theta]_{MRW}$. Samples were dialyzed into 200 mM NaF, 20 mM NaH_2PO_4/NaOH, pH 7.2. Full spectra (260 to ~180 nm; dynode voltage <500 V) were collected at protein concentrations of ~0.5 mg/ml in a 0.02-cm quartz cuvette at 4 °C. Concentrations were determined by absorption at 280 nm, assuming an extinction coefficient of $\epsilon_{280} = 25{,}940\ M^{-1}\ cm^{-1}$, based on the amino acid composition (35). CD spectra were deconvoluted to determine secondary structure content with the CDsstr algorithm (36), as implemented in the Dichroweb server (37) with the reference data sets SP175 (190–260 nm) (38) and 3 (185–260 nm) (39). Thermal transition curves were constructed from spectra recorded in a 0.1-cm cell (protein concentration ~0.1 mg/ml) at various temperatures between 4 and 85 °C upon stepwise heating. Ellipticities $[\Theta]$ observed at 200, 207, and 218 nm as a function of temperature were normalized to the fraction of folded protein, $F = ([\Theta] - [\Theta]_u)/([\Theta]_n - [\Theta]_u)$, where $[\Theta]_n$ and $[\Theta]_u$ represent signals for the fully folded and fully unfolded species, respectively. Data were fitted assuming a two-state transition (40) with the melting temperature, T_m, defined as $F(T_m) = 0.5$.

Surface Plasmon Resonance (SPR)-based Binding Assay—Real time binding analyses were performed on a Biacore 3000 apparatus, operated by a Biacore 3000 control software 4.1 version (Biacore Sweden). HS (average mass = 15 kDa; Celsus Laboratories; Cincinnati, OH) was biotinylated at the reducing end, as described previously (41), and immobilized on a CM4

Biacore sensorchip. Briefly, two flow cells were activated with 50 μl of 0.2 M *N*-ethyl-*N*′-(diethylaminopropyl)-carbodiimide and 0.05 M *N*-hydroxysuccinimide. Next, 50 μl of streptavidin (Sigma) at 0.2 mg/ml in 10 mM sodium acetate buffer, pH 4.2, was injected. The remaining activated groups were blocked with 50 μl of 1 M ethanolamine, pH 8.5. Typically, this procedure allowed coupling of ~2500 response units of streptavidin on both flow cells. Biotinylated HS (15 μg/ml) was then injected over one surface (until achieving a level of 50 response units), and the other surface remained untreated to serve as a negative control. Before use, the chip was submitted to several injections of 2 M NaCl and washed in a continuous flow of 10 mM Hepes, pH 7.4, 0.15 M NaCl, 0.05% P20 detergent. For binding assays, WT or mutant α3LG45 was injected over both negative control and HS surfaces for 5 min at 25 °C at a rate of 50 μl/min. The HS surface was regenerated with a 1-min pulse of 0.05% SDS followed by a 2-min pulse of 2 M NaCl. Apparent dissociation constants were estimated by fitting the steady state values at equilibrium $R_{eq}(c)$ assuming one or two binding sites with $R_{eq}(c) = R_{eq}^{max}/(K_D + c)$ and $R_{eq}(c) = R_{eq}^{max1}/(K_{D1} + c) + R_{eq}^{max2}/(K_{D2} + c)$, respectively.

Molecular Modeling—A three-dimensional model of the α3LG45 domain pair was generated with ProMod II (Version 3.70 SP3 (42)). The x-ray derived coordinates of mouse LN α1 LG45 (Protein Data Bank code 2JD4, chain B (43)) served as a template. After optimizing the alignment manually, a final total energy of −7025 kJ/mol was achieved.

RESULTS

Production and Purification of Recombinant α3LG45-His_6 Proteins—The α3LG45 fragment was produced as described previously (29) except that a His_6 tag was added at the C terminus. Transfected human embryonic kidney 293-EBNA cells secreted LG45-His_6 protein into the culture medium. We tested the effect of the His_6 tag on the ability of recombinant LG45-His_6 to bind heparin. As shown in Fig. 1*A*, the protein was captured on heparin-Sepharose beads and was released with 1 M NaCl buffer. Purification was based on His_6 tag binding to Ni-NTA-conjugated beads, followed by elution with an imidazole buffer. SDS-PAGE analysis of untagged and His_6-tagged LG45 proteins revealed a slight difference in the migration of the two proteins (Fig. 1*B*).

To test whether specific arginine and lysine residues in the α3LG45 domains are involved in heparin and syndecan binding (Fig. 1*C*), we substituted these charged residues with glutamine. The side chain volume and hydrophilicity are more closely related to the basic residues than the alanine typically used in substitution studies (43–46). First, we designed a series of single or double mutant proteins (Fig. 1*D*, *mutants 1–12*). Then we designed a second series that included triple mutants (mutants 13–18). Residues were selected based on sequence alignments among homologous human LN isoforms. We mutated all residues that were shown to participate in heparin binding in the α1 chains (43, 44) and α4 chains (46). Residues Lys-1387 and Arg-1389 were mutated (mutant 1), because the corresponding residues in the α1 and α2 chains have been shown to be involved in syndecan-1 binding (47). Lys-1421 (mutant 4) and Arg-1423 (mutant 5) were mutated because these residues have previously been shown to affect heparin and cell binding based on a synthetic peptide approach (24), although the Lys-1421 residue is substituted with acidic residues in the mouse and rat α3 chains. Double and triple mutant proteins 13 and 14 cover simultaneous mutations of the lysine residues within the synthetic peptide A3G75aR reported as responsible for syndecan-2- and -4-mediated cell binding activity (23). Finally, Arg-1436, Lys-1438, Lys-1497, and Lys-1613 (located in LG5), were mutated because these were identified as heparin-binding residues in a study where native α3LG45 was cross-linked to heparin beads, and the sequences involved were characterized (22). WT LG45 and all mutated LG45 proteins were expressed in 293-EBNA cells and secreted into the culture medium. They were purified using Ni^{2+}-chelated beads. Each mutated protein migrated as a major band, displayed a molecular mass equivalent to that of WT, and gave a strong signal when probed in immunoblots with the anti-LG45 pAb (Fig. 1*D*).

α3LG45 and Mutant Protein Binding to Heparin and HS—The binding properties of WT and mutated LG45 were tested on a heparin Hitrap column. We started with low ionic strength to determine the NaCl concentrations required for displacement (Table 1). As the His_6 tag did not affect the heparin binding properties of LG45, this system was suitable for testing the properties of mutant LG45 proteins. The analysis of proteins 1–14, including single, double, and triple mutants (Fig. 1*D*), revealed that two proteins carrying a single mutation (Arg-1436 or Lys-1438) eluted from the column at a much lower ionic strength (0.48 M NaCl) than the WT α3LG45 (0.65 M NaCl). This suggested that this sequence might harbor a major binding site. Four mutants behaved identically to the WT protein, but six other mutants eluted at 0.6 M NaCl suggesting that additional residues may also participate, to a lesser extent, in GAG interactions. Combining mutations of two or three of these low binding residues (*mutants 13* and *14*, Fig. 1*D*) only slightly modified the ionic strength to 0.55 M NaCl. Therefore, a series of double and triple mutants was designed to target the sequence ^{1433}KKLRIKSKEK, which harbors residues Arg-1436 and Lys-1438 (Fig. 1*D*, *lower panel*). These mutants displayed severe defects in heparin binding. When both the Arg-1436 and Lys-1438 residues were mutated, the defect in heparin binding was only moderately intensified, 0.44 M NaCl being necessary for elution. When a neighboring residue, Lys-1434, was mutated, the mutant protein eluted at 0.54 M NaCl. When all three residues were combined, Lys-1434/Arg-1436/Lys-1438, the mutant eluted at a NaCl concentration of only 0.41 M. In contrast, another combination mutant, Arg-1436/Lys-1438/Lys-1440, eluted at the same NaCl concentration required for eluting the Arg-1436/Lys-1438 mutant. These data suggest that the residues Lys-1434, Arg-1436, and Lys-1438 were critical for heparin binding of the LG45 domain. As the binding to heparin was not fully abolished with any of the mutated LG45 proteins, we used SPR spectroscopy to analyze the WT and mutated LG45 interactions with HS. First, we determined the affinity of WT LG45 for HS using biotinylated HS immobilized on a streptavidin-coated sensor chip. This system mimicked to some extent cell membrane-anchored HSPG. We injected a range of concentrations (8.7–100 nM) of LG45 to measure binding (Fig. 2*A*). The association phase (from 150 to 450 s) was

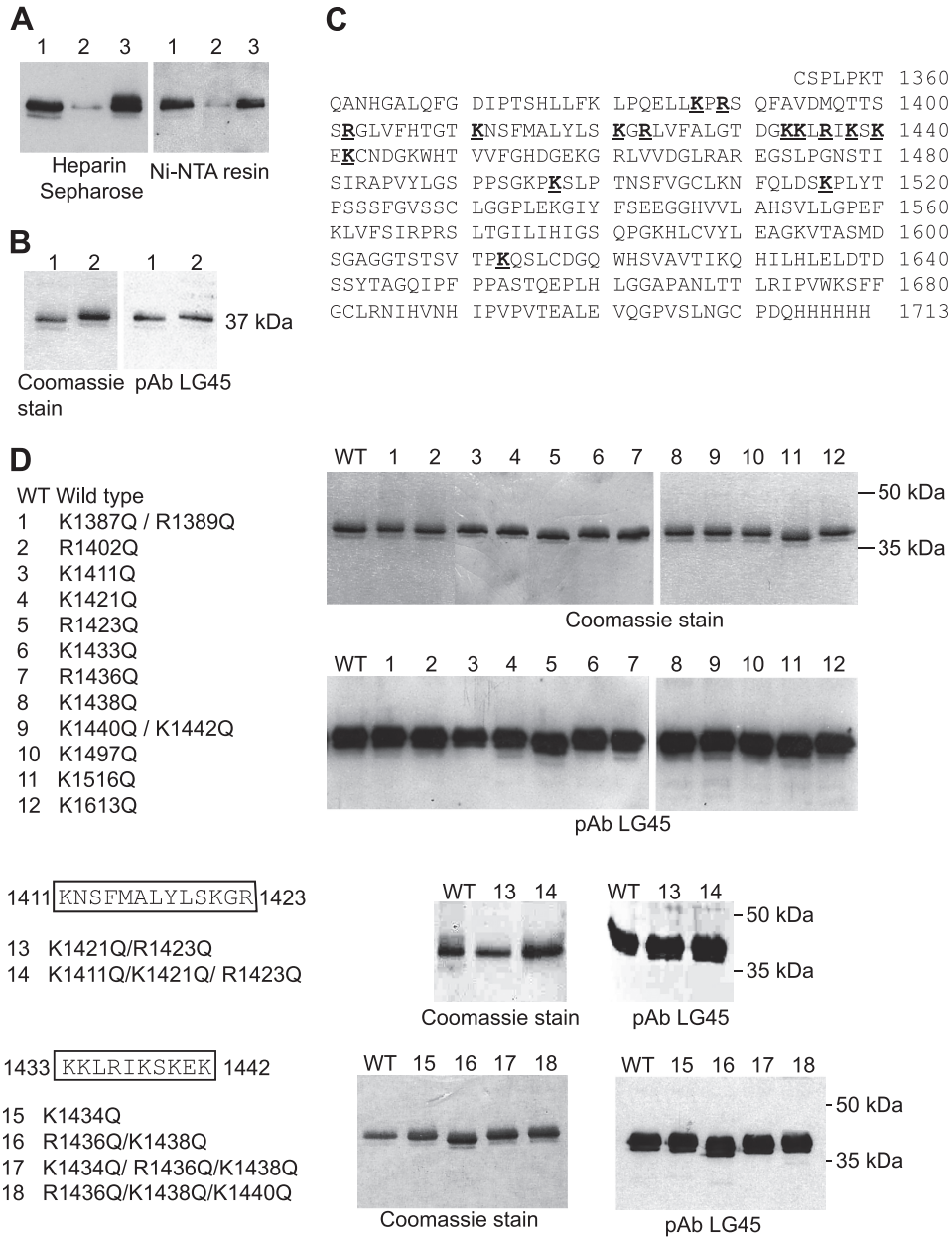

FIGURE 1. **Recombinant α3LG45-His$_6$ proteins.** *A, left panel,* 2 ml of serum-free, 293-EBNA-conditioned cell culture medium (*lane 1*) were mixed with heparin-Sepharose beads and analyzed for its content of LG45-His$_6$ (*lane 2*). Proteins were eluted with 100 μl of 0.02 M Tris-HCl, pH 7.4, 1 M NaCl (*lane 3*). *Right panel,* serum-free, 293-EBNA-conditioned cell culture medium (*lane 1*) was mixed with Ni-NTA-conjugated beads and analyzed for its content of LG45-His$_6$ (*lane 2*). Proteins were eluted with 100 μl of PBS with 200 mM imidazole (*lane 3*). All samples (20 μl) were separated by 12% SDS-PAGE under reducing conditions, and blots were probed with the pAb LG45. *B,* comparison of recombinant untagged LG45 (*lanes 1*) and LG45-His$_6$ (*lanes 2*) proteins visualized by Coomassie Brilliant Blue R-250 (2 μg) or immunoblotting (0.15 μg) with pAb LG45. The position of a 37-kDa molecular mass marker is shown on the *right*. *C,* amino acid sequence of the WT α3LG45-His$_6$ recombinant fragment; residues substituted with glutamine in the mutants are shown in *bold* and *underlined*. *D,* WT and mutated recombinant α3LG45-His$_6$ proteins (single, double, and triple mutations as indicated on the *left*) were expressed in 293 EBNA cells and purified with Ni^{2+}-chelated beads. Purified proteins were analyzed by SDS-PAGE and either stained with Coomassie Blue or immunoblotted with the anti-LG45 pAb, as indicated.

allowed to proceed to equilibrium. Both the association and dissociation ($t > 450$ s) kinetics indicate a complex interaction mechanism with a fast phase followed by a slower one, which is especially obvious by the long time required to reach base-line levels after protein injection stopped. This behavior probably reflects the heterogeneity of the HS preparation with respect to length and sulfation pattern. To reduce bias in deriving affinity data from rate constants, we focused on establishing steady state values at equilibrium. R_{eq} as a function of protein concentration was fitted assuming one or two binding sites resulting in high affinity dissociation constants of ~10 and ~6 nM, respectively, indicating that WT LG45 displayed a strong affinity for HS (Fig. 2*B*).

The same assay was used to determine the HS binding strength of the different LG45 mutants (Fig. 2*C*). We injected WT or mutant LG45 proteins (all at 13 nM) over the HS surface. The binding responses of the mutants were compared with that of WT LG45. The binding to HS was slightly different as compared with that observed with heparin (Fig. 2*C*). Although only two mutated LG45s showed affinity equivalent to the WT, sev-

TABLE 1
Mapping of ligand-binding sites on α3LG45 by mutagenesis
Values are the mean of three independent determinations.

Laminin α3 LG45 mutant	Heparin binding[a] (M NaCl)	Syndecan-1 binding[b]	Syndecan-4 binding[c]
Wild type	0.65[d]	1.00	1.00
K1387Q/R1389Q	0.65	0.97	0.94
R1402Q	0.60	1.05	1.02
K1411Q	0.60	1.01	1.12
K1421Q	0.60	1.02	1.09
R1423Q	0.60	1.03	0.92
K1421Q/R1423Q	0.55	0.98	1.01
K1411Q/K1421Q/R1423Q	0.55	0.97	0.95
K1433Q	0.65	0.98	1.06
R1436Q	0.48	0.71	0.80
K1438Q	0.48	0.73	0.72
K1440Q/K1442Q	0.60	0.94	0.21
K1497Q	0.60	0.98	1.15
K1516Q	0.65	1.04	0.93
K1613Q	0.65	1.02	0.94
K1434Q	0.54	0.83	0.87
R1436Q/K1438Q	0.44	0.45	0.34
K1434Q/R1436Q/K1438Q	0.41	0.07	0.23
R1436Q/K1438Q/K1440Q	0.44	0.26	0.02

[a] Concentration of NaCl required for elution from a heparin affinity column equilibrated in 0.02 M Tris-HCl, pH 7.4.
[b] As determined by solid phase assay with antibodies against syndecan-1 and relative to wild type binding.
[c] As determined by solid phase assay with antibodies against syndecan-4 and relative to wild type binding.
[d] Untagged LG45 required 0.65 M NaCl for elution from heparin.

eral mutants showed a 20–35% affinity decrease. Among these, K1411Q, K1421Q, and R1423Q mutants displayed equivalent binding to HS even when they were combined. In contrast with the heparin binding studies, the Lys-1440/Lys-1442 mutant showed a 50% decrease in binding to HS. The three Lys-1434, Arg-1436, and Lys-1438 mutants each displayed an equivalent 60% binding that dropped to 10% when mutated Arg-1436 and Lys-1438 were combined confirming the importance of these residues. The two triple mutants, Lys-1434/Arg-1436/Lys-1438 and Arg-1436/Lys-1438/Lys-1440, failed to bind to HS, confirming that LG45 encompasses a unique major site for HS binding.

Structure and Stability of α3LG45 and Mutant Proteins—To ensure that mutations did not impact on heparin binding through incorrect protein folding, all protein variants were analyzed by CD spectroscopy. Far-UV CD spectra were recorded for wild type α3LG45 and all mutant fragments (Fig. 3*A*). Within the 260 to 190-nm range, all spectra were identical within experimental error. No significant changes were observed between 4 and 45 °C. The spectra showed a characteristic minimum at 218 nm and maxima at 201 and 189 nm, which was consistent with data reported for the proteolytically derived fragment E3 from mouse tumor laminin-111 that comprised the α1LG45 domains (48). Deconvolution of the spectra showed that the α-helix and β-strand contents were 2–4 and 40–44%, respectively. This agreed with the 1.2% α-helix and 46.9% β-sheet contents found for the x-ray-derived structure of the mouse α1LG45 domain pair (Protein Data Bank code 2JD4, see Ref. 43). When heated above 45 °C, the CD signal indicated unfolding of the LG45 domains (Fig. 3*B*), which was not reversible upon cooling. Assuming a two-state transition, data fitting resulted in apparent melting temperatures between 57.5 and 59.2 °C. The CD spectra and the thermal stability indicated that α3LG45 and all mutant proteins had very similar conformations consistent with the x-ray-derived structures of laminin LG domains (43, 45, 49).

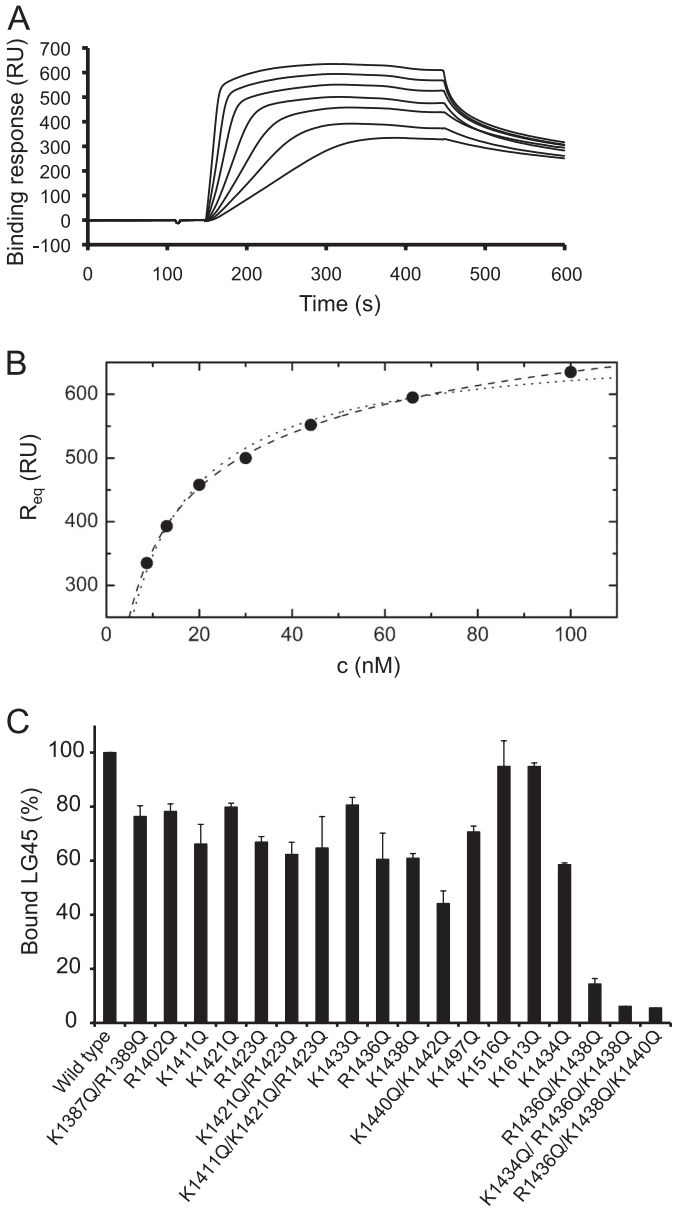

FIGURE 2. **SPR analysis of HS binding to WT and mutated LG45-His$_6$.** *A,* series of sensorgrams showing the binding of different concentrations of the WT LG45 to immobilized HS. LG45 concentrations of (from *top to bottom*) 100, 66, 44, 30, 20, 13, and 8.7 nM were injected for 5 min over control and HS-activated surfaces at a flow rate of 50 μl/min. The response (in response units) was recorded as a function of time. Control sensorgrams were subtracted from HS sensorgrams. *B,* equilibrium binding data R_{eq} as function of concentration. R_{eq} are the steady state values at equilibrium recorded at the end of the association phase, and *c* indicates the concentrations of injected α3LG45. *Dotted* and *dashed lines* represent fitting of the data assuming one or two binding sites with $K_D = 9.6 \pm 0.6$ nM ($r^2 = 0.991$, $\chi^2 = 124$), and $K_{D1} = 6.1 \pm 1.6$ and $K_{D2} = 110 \pm 13$ nM ($r^2 = 0.999$, $\chi^2 = 17$), respectively. Experiments were performed in triplicate. *C,* WT and mutant LG45 protein (13 nM) binding responses recorded at the end of the injection phase. The results (means of three experiments ± S.D.) are expressed as the percentage binding relative to the WT response (100%).

α3LG45 and Mutant Protein Binding to Syndecan-1 and -4—We previously showed that cell adhesion to the α3LG45 fragment relies on the HSPG receptor syndecan-1 without involvement of syndecan-4 (29, 30). In several cell types, including

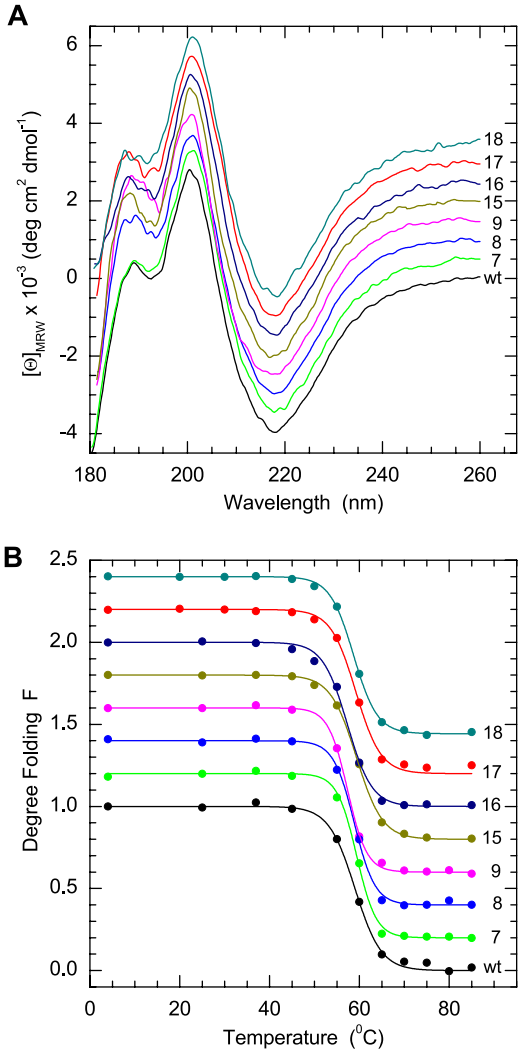

FIGURE 3. **CD spectra and thermal stability of α3LG45 WT and mutant proteins.** *A,* far-UV CD spectra were recorded at 4 °C for the protein samples (numbers indicated on the *right* correspond to those shown in Fig. 1*D*). Spectra were staggered by successive addition of +500 degrees cm^2 $dmol^{-1}$, *i.e.* the signal at ~260 nm is around zero for all proteins. *B,* thermal transition curves were derived from full spectra. Data points represent the mean values of the degree of folded protein F, as defined under "Experimental Procedures," observed at 200, 207, and 218 nm. *Lines* represent fits assuming a two-state transition. To facilitate comparisons, data are staggered by +0.2 units.

NHK and HT1080 cells, the syndecan-1 receptor induced, in an integrin-independent manner, the formation of filopodium-like protrusions (29–31). We therefore used this model to investigate whether the various mutations could affect the syndecan-1 interaction. Cell adhesion assays were performed with HT1080 cells as these cells are more easily dissociated from culture plates with EDTA. We found that the different heparin affinities of α3LG45 proteins correlated well with syndecan-1-mediated cell adhesion. HT1080 cells displayed similar adhesion when placed on WT LG45 and all mutant LG45 proteins that required either 0.65, 0.6, or 0.55 M NaCl concentrations for elution from heparin (Fig. 4*A*). Only cell adhesion to the Arg-1436 and Lys-1438 mutants (0.48 M NaCl) was decreased. The analysis of cell phenotypes (Fig. 4*B*) revealed that cells plated on all mutants, except Arg-1436 and Lys-1438 mutants, spread and formed protrusions in a manner comparable with cells plated on the WT protein (60–70% of adhered HT1080 cells developed microspikes). The cells plated on Arg-1436 and Lys-1438 mutants failed to form protrusions (only 2% of adhered cells developed protrusions) and were clustered in aggregates. We then performed a dose-response analysis of cell adhesion to the mutants that targeted the sequence ^{1433}KKLRIKSKEK (Fig. 4*C*). This confirmed that Lys-1434, Arg-1436, and Lys-1438 were crucial for syndecan-1-mediated cell adhesion, and protrusion elongation required residues Arg-1436 or Lys-1438. Indeed, the single Lys-1434 mutant displayed reduced cell adhesion, equivalent to that observed with the Arg-1436 and Lys-1438 mutants, but Lys-1434 also formed protrusions. Cells failed to adhere to the Lys-1434/Arg-1436/Lys-1438 triple mutant at all concentrations tested. Moderate but equivalent adhesion was obtained with either the Arg-1436/Lys-1438 or Arg-1436/Lys-438/Lys-1440 mutants. This suggests that the Lys-1440 residue mutation did not affect -mediated cell adhesion.

As other studies have shown that syndecan-4 can interact with α3LG45 (23, 24), we investigated whether syndecan-1 and -4 extracted from cell lysates can interact with LG45 through the same binding site. First, we used solid phase assays to test WT and mutated LG45 proteins immobilized on nickel-chelate plates with solubilized syndecan-1 and -4 derived from human keratinocyte (HaCat) cells that express significant amounts of syndecan-1 and -4 (Table 1) (29). The first series of mutants (*mutants 1–14*, Fig. 1) revealed that both Arg-1436 and Lys-1438 mutants displayed a 20–30% reduced affinity for syndecan-1 and -4. In contrast, all the other mutants were comparable with WT LG45 in binding syndecan-1 and -4. Unexpectedly, the Lys-1440/Lys-1442 mutant was deficient in syndecan-4 binding as a residual 20% interaction could be detected. The second series of mutants (*mutants 15–18*, Fig. 1) revealed that syndecan-1 failed to bind the Lys-1434/Arg-1436/Lys-1438 mutant, which confirmed our syndecan-1-mediated HT1080 cell adhesion data. Interestingly, syndecan-4 moderately interacted with the Lys-1434/Arg-1436/Lys-1438 mutant, but failed to bind to the Arg-1436/Lys-1438/Lys-1440 mutant. These results suggest that, although Lys-1440 was apparently not essential for syndecan-1 binding, it was critical for syndecan-4 binding. We tested this hypothesis by affinity precipitation (pulldown) experiments (Fig. 5, *A* and *B*). HaCat cell lysates were mixed with nickel magnetic beads coated with WT or mutated LG45 proteins. Beads were subjected to heparitinase/chondroitinase ABC treatment, and gel sample buffer was added to the samples prior to their electrophoresis analysis so that all bound syndecan-1 and -4 could be detected. Western blot analysis revealed bands that corresponded to syndecan-1 or syndecan-4 (Fig. 5*A*) core proteins in the material bound to the WT and mutant LG45 proteins. Consistent with the solid phase assays, the Arg-1436/Lys-1438 mutant showed important defects in both syndecan-1 and syndecan-4 binding; syndecan-1 failed to interact with the Lys-1434/Arg-1436/Lys-1438 mutant, whereas syndecan-4 failed to bind the Arg-1436/Lys-1438/Lys-1440 mutant. The experiment was repeated using NHK and HT1080 cells (Fig. 5*B*) with the most relevant mutated LG45 proteins and produced similar results. These results show that syndecan-1 and syndecan-4 share a common

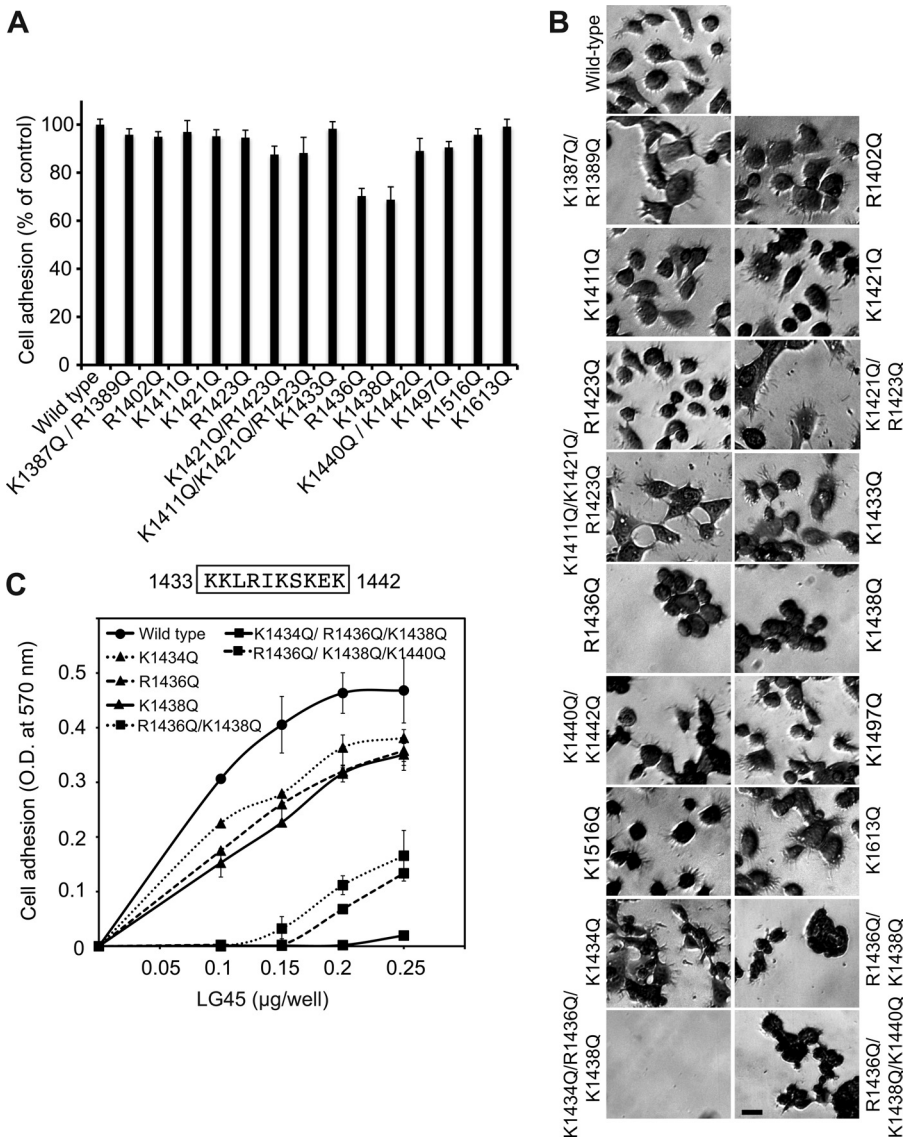

FIGURE 4. **Cell adhesion on WT and mutated α3LG45.** Mutated LG45 proteins were analyzed for their capacity to induce syndecan-1-mediated HT1080 cell adhesion. The extent of cell adhesion was measured with a colorimetric assay as described under "Experimental Procedures" and expressed as a percentage of the total cell adhesion observed on WT LG45. Data are representative of three independent experiments. *A,* multiwell Ni^{2+}-chelate plates were coated with WT and mutated LG45 (0.2 μg). HT1080 cells that expressed syndecan-1 receptors were seeded (8×10^4 cells/well) onto the plates and incubated for 30 min. *B,* phase contrast micrographs show morphology of cells that adhered to WT and LG45 mutants. Photographs were taken after 30 min incubation. *Bar,* 50 μm. *C,* multiwell nickel-chelate plates were coated with WT and LG45 proteins specifically mutated in the targeted Lys-1434 to Lys-1440 region. HT1080 cells that expressed syndecan-1 receptor were seeded (8×10^4 cells/well) onto the plates and incubated for 30 min.

binding site that includes residues Arg-1436 and Lys-1438 in LG45.

Syndecan-4 Binding to LG45 Involves Both HS and the Core Protein—The LG45/syndecan-1 interaction was previously shown to rely exclusively on GAGs with a participation of both HS and CS (29). To study the mechanism of syndecan-4/LG45 binding, intact as well as HS-free GAGs from cells were compared to reveal the role of HS in syndecan-4 binding (Fig. 5*C*). NHK and HT1080 cells were either untreated or treated with heparitinase I to degrade HS. WT and mutated LG45 proteins immobilized on nickel-chelate plates were incubated with solubilized intact or enzyme-treated cell lysates, and bound syndecan-4 was detected by ELISA. Treatment of the cells with heparitinase I only partially prevented interaction of the syndecan-4 with LG45 suggesting another binding mechanism. Although HS digest only moderately decreased syndecan-4 interaction with the tested mutants, it completely abrogated the residual interaction observed with the Lys-1440/Lys-1442 mutant. As shown in Fig. 5*C* (*right panel*), heparitinase I digest was efficient as HS were not detected in the heparitinase I-treated lysates. To further evaluate the binding of the syndecan-1 and -4 core proteins to LG45, we produced fusion proteins between GST and the human syndecan-1 and -4 ectodomains (GST-hS1ED and GST-hS4ED respectively). The fusion proteins were purified on glutathione-Sepharose beads and analyzed by SDS-PAGE followed by Coomassie Blue staining (Fig. 5*D*). The GST-hS1ED and GST-hS4ED were then immobilized on glutathione plates and tested for their ability to interact with soluble LG45 protein. As shown in Fig. 5*D*, LG45 was detected only in wells coated with GST-hS4ED reinforcing the

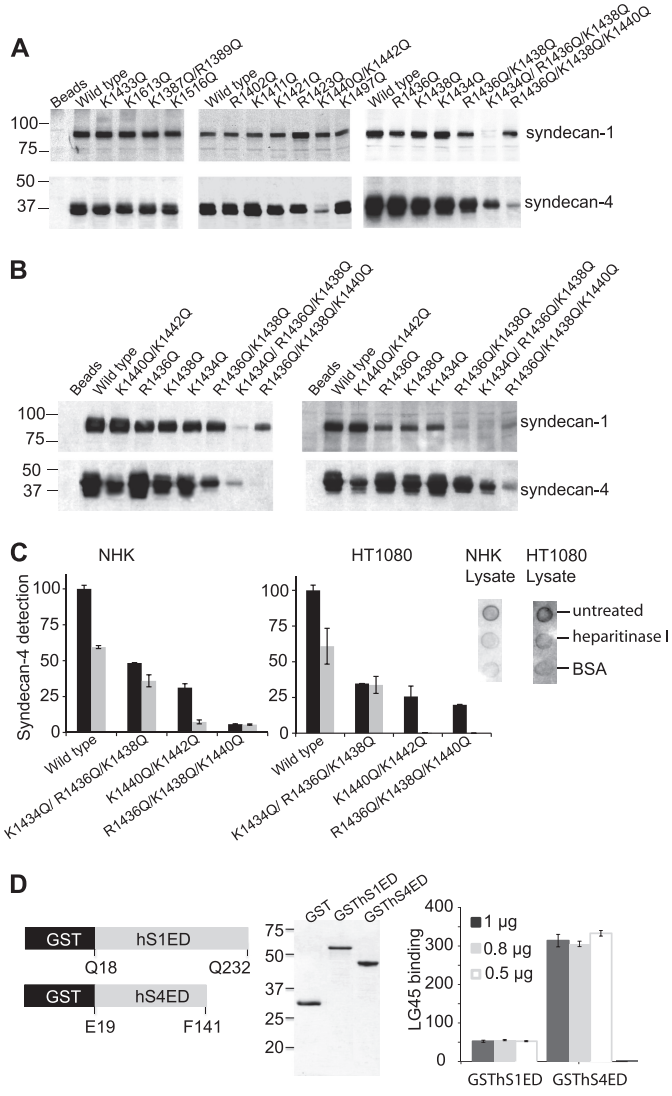

FIGURE 5. **Syndecan-1 and -4 binding to WT and mutated α3LG45 proteins.** *A* and *B,* HaCat, NHK, and HT1080 cell lysates were incubated with beads coated with WT or mutated LG45 proteins as indicated. Uncoated beads were used as a control. After washing, beads were digested with heparitinase I and chondroitinase ABC and prepared for electrophoresis analysis. The bound material was analyzed on an 8 or 10% SDS-polyacrylamide gel under reducing conditions followed by immunoblotting with the pAb H-174 against syndecan-1 or a pAb against syndecan-4 as indicated. *A,* HaCat lysates were incubated with beads covered with each individual mutated LG45 protein; *B,* NHK and HT1080 lysates were incubated with selected LG45 mutants as indicated. The migration positions of molecular weight markers are shown on the *left*. The data are representative of three independent experiments. *C,* effect of GAGs on syndecan-4 binding to WT and mutated LG45 proteins. NHK (*left panel*) and HT1080 cells (*right panel*) were collected from culture plates in digestion buffer, followed by treatment with (*gray bars*) or without (*black bars*) 8 milliunits/ml heparitinase I for 4 h at 25 °C. After treatment, cell extracts were lysed in RIPA buffer, and syndecan-4 ELISA-based assays were performed with 96-well nickel-chelate plates, coated with WT or mutated LG45-His_6, as described under "Experimental Procedures." Results are expressed as a percent of syndecan-4 interaction with the WT LG45 in the absence of enzyme treatment. *Right panel,* nitrocellulose containing BSA and lysates of heparitinase I-treated and untreated -NHK and HT1080 cells (1 μg) were immunoblotted with the anti-HS F58–10E4 mAb. *D, left panel,* schematic representation of the GST-fused human syndecan-1 and -4 ectodomains. *Central panel,* 15% SDS-PAGE analysis followed by Coomassie Blue staining of 0.5 μg of each GST fusion protein, including the GST alone (as indicated). *Right panel,* GST-fusion proteins were coupled to glutathione-chelate 96-well plates and incubated with soluble LG45. After washes, bound LG45 was detected as described under "Experimental Procedures."

hypothesis that the syndecan-4 core protein participates in the binding to LG45.

Effect of WT and Mutant LG45 on Keratinocyte Migration—A study reported that LG45 could stimulate NHK migration when added to the culture through a mechanism involving syndecan-4 (26, 27). Therefore, we tested whether mutation in the syndecan-4-binding site could affect this phenomenon. We directly assessed the migratory behavior of NHKs by monitoring cell migration for 8 h with a time-lapse video recorder. The individual cell tracks (Fig. 6*A*) showed marked differences in behavior when WT α3LG45 was absent or present in the culture medium. Maximal relative distances to the origin measurements revealed that 80% of cells plated in the absence of LG45 covered distances less than 50 μm; in contrast, 65% of cells plated with WT LG45 covered 50–200 μm ($n = 100$ cells, $p < 0.001$; Fig. 6*B*). Interestingly, the mutant protein deficient in syndecan-4 binding (Arg-1436/Lys-1438/Lys-1440) failed to trigger NHK motility. These results confirm previous findings showing that soluble LG45 stimulate NHK migration and further show that residues Arg-1436/Lys-1438/Lys-1440 are involved in this phenomenon.

DISCUSSION

Unique HS Binding Domain within α3LG45 Harbors Specific Syndecan-1- and -4-binding Sites—This study demonstrates that the α3LG45 domain of LN332 harbors a major HS binding region (^{1433}KKLRIKSKEK) that was different from any sequences previously identified through synthetic peptide screening (20, 23, 50). Thus, in this case, short peptides could not reproduce the structural conformation assumed by this region within the full-length protein. Interestingly, the sequence identified in this study was identical to one of the three HBDs identified by Vivès *et al.* (22). We performed a more detailed analysis, which revealed that three critical residues (Lys-1434, Arg-1436, and Lys-1438) were involved in syndecan-1 interaction. In addition, we found that syndecan-4 could bind a region in LG45 that was different from that recognized by syndecan-1. A mutant encompassing residues Lys-1440 and Lys-1442 displayed major defects in syndecan-4 interaction suggesting an important role for this region, and we suggest that this region may encompass the syndecan-4 core protein binding domain. We further showed that Arg-1436, Lys-1438, and Lys-1440 are the key residues involved in the syndecan-4 interaction. Taken together, our results show that syndecan-1 and syndecan-4 bind to distinct but overlapping sites, with a common region including residues Arg-1436 and Lys-1438. Each site contains additional specific residues located N- or C-terminal to these two central residues.

Specific residues involved in heparin, dystroglycan, syndecan, and calcium binding have been identified by site-directed mutagenesis for the LG4 or LG45 domains of the laminin α1, α2, and α4 chains and corroborated by x-ray structural analysis for α1 and α2 (43–46). Our results show that the cluster of basic residues (Lys-1434 to Lys-1438) in α3LG4 that were responsible for heparin and syndecan-1 and -4 binding (Table 1) correspond to similar clusters identified in the α1 and α4 chains (Fig. 7*A*). The α2 chain has no basic residues within this sequence region. Instead, the α2LG5, rather than the α2LG4, domain

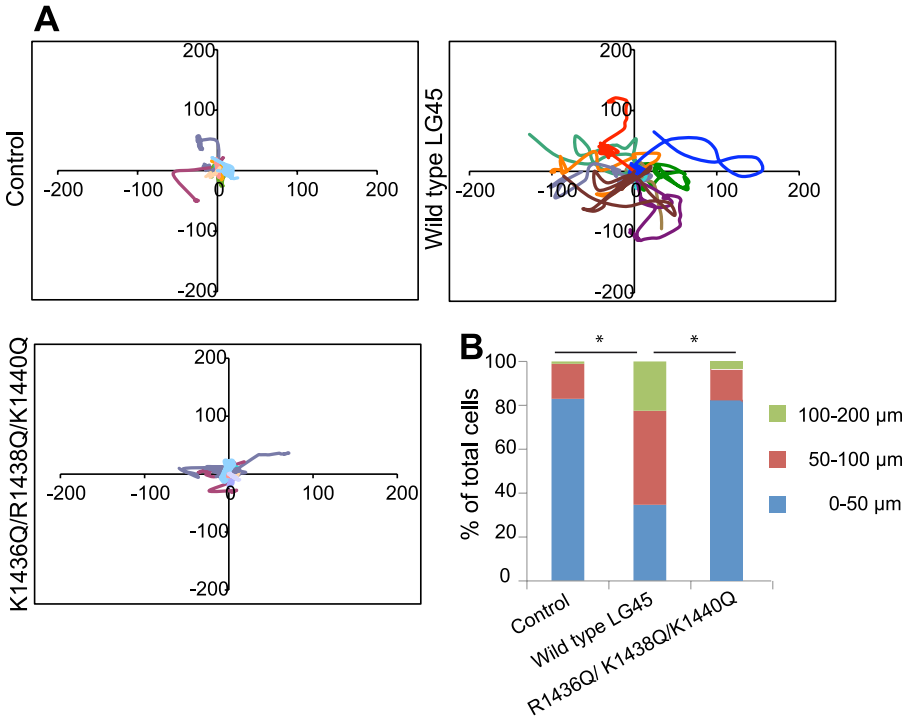

FIGURE 6. **Effect of WT and mutated α3LG45 proteins on keratinocyte migration.** *A,* NHKs were seeded at 10^4 cells/well in KBM-2 medium alone (control) or KBM-2 medium that contained either WT or mutated LG45-His_6 (20 μg/ml). Cell migration was recorded at 20-min intervals over a period of 8 h. In each condition, the cell migratory plot shows positions for 15 cells in one field, oriented to place the cell origins at *x*(0), *y*(0). The distance migrated in micrometers is indicated on the *axes*. *B,* histograms of maximal relative distances to origin data for 100 cells in each condition. Total data corresponding to migrated distances were compared with the Student's *t* test (*, $p < 0.001$ between control and WT LG45 and between WT and R1436Q/K1438Q/K1440Q).

appears to be responsible for heparin binding (49, 51). Lysine and arginine residues are also found in the equivalent positions of the α3 chains of mouse, rat, chicken, and frog (*Xenopus tropicalis*). Mutations of Lys-1440 and Lys-1442 had no significant effect on the binding to heparin or syndecan-1 but led to markedly reduced binding to syndecan-4 (Table 1). The α4LG4 lysine residue, which corresponds to Lys-1442 (Fig. 7*A*), was partially involved in heparin binding, but the mutant was not tested for syndecan interactions (see Table 1 in 46). For known α3 chains, including rat, mouse, chicken, and frog, residues in the position equivalent to Lys-1442, but not Lys-1440, are either lysine or arginine, which indicates potential functional importance.

Syndecan-1 and -4 Binding Domains Are Juxtaposed and Both Accessible—A homology-based structural model of the human α3LG45 domains with the mouse α1LG45 crystal structure as a template (43) showed that the residues involved in heparin binding were located on the outer edge of β-strand G (see nomenclature accompanying Ref. 49), although residues involved in syndecan-4 binding were within the adjacent loop that connects strands G and H (Fig. 7*B*). Strand G forms the outer edge of the concave β-sheet of the β-sandwich structure. We identified an additional group of mutants that also contributed to heparin binding as they were eluted at 0.6 M NaCl. SPR analysis of the interactions between these mutants and HS confirmed these findings and identified Arg-1402, Lys-1411, Lys-1421, Arg-1423, and Lys-1497 as low GAG affinity residues. The structural model suggests that the concave surface of the β-sheet might act as a groove to align GAG chains along low affinity residues and direct them toward Arg-1436 and Lys-1438. A surface view of this structure (Fig. 7*C*) shows that the NH_2 groups of the basic residues involved in heparin and syndecan binding are accessible.

In addition to site-directed mutagenesis studies of the LN LG domains (43–46, 49), short synthetic peptide studies have elucidated heparin- and syndecan-binding sites. Peptide A3G75aR, which harbored residues ^{1412}NSFMALYLSKGR of human α3LG45, was found to bind to heparin and promote cell adhesion through syndecan-2 and -4 (23). Another report described a heparin-binding synthetic peptide ^{1399}KPRLQFSLDIQT of the mouse α3LG4 sequence corresponding to residues 1387–1398 of human α3LG4 (Fig. 1*C*) (20). We made mutant α3LG45 proteins that had substitutions of Lys-1387/Arg-1389, Lys-1421, or Arg-1423 with glutamine; however, these showed no effects on syndecan-1 or -4 binding (Table 1 and Fig. 5). Similar discrepancies between alternative approaches were also found for HBDs within the LG domains of the α1, α2, and α4 LN chains (*cf.* Fig. 7*A* with Fig. 7 of Ref. 52). This probably indicates that binding required a specific spatial arrangement of the functional amino acid side chains, which cannot be adopted within a short peptide.

This study reveals that the GAG chains of syndecan-1 and -4 expressed by NHK interact with specific residues in LG45. It shows that residues Arg-1436/Lys-1438 participate in both syndecan-1 and -4 binding, although residues Lys-1434 and Lys-1440 are specific for binding to syndecan-1 and -4, respectively. This is the first study to demonstrate this type of specificity in syndecan binding in any LN or other ECM protein. It has long been suspected that specific sulfation patterns are required for specific HS/ligand interactions, and the overall structure of the

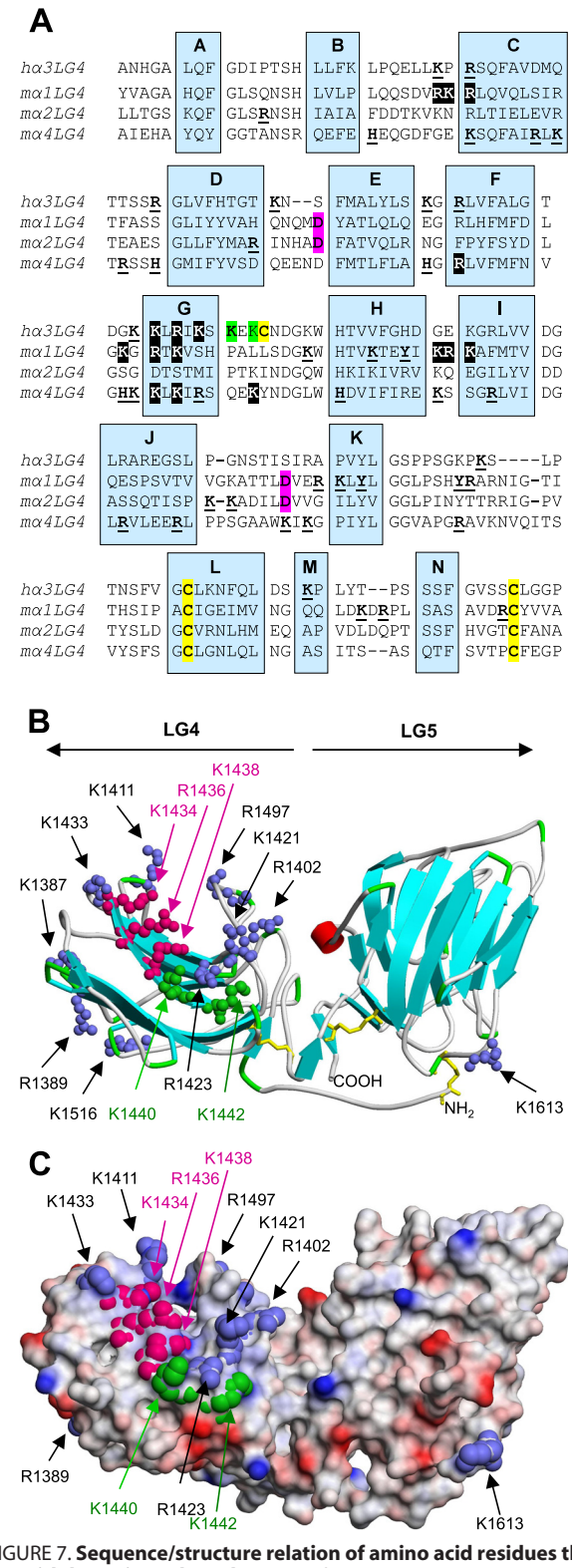

FIGURE 7. **Sequence/structure relation of amino acid residues that interact with heparin and syndecans.** *A,* human LN α3LG4 sequence (residues 1362–1534) was aligned to that of mouse LN α1LG4 (residues 2718–2898; accession number P19137), LN α2LG4 (residues 2755–2934; accession number Q60675), and LN α4LG4 (residues 1457–1636; accession number P97927). Residues that diminished heparin binding activity when mutated to glutamine (α3) or alanine (α1, α2, and α4), are shown in *white on a black background*. Other basic residues that could be mutated with no significant effect on heparin binding are shown in *bold* and *underlined*. Residues in the α3 chain that affected syndecan-4, but not heparin binding, are highlighted in *green*. Aspartic acid residues involved in Ca^{2+} binding are highlighted in *purple*. All cysteine residues are highlighted in *yellow*. Mutation data were reproduced from previous studies for the α1 (43, 44), α2 (45), and α4 chains (46). The assignment to β-strands *A–N* (*boxed*), using the nomenclature of Tisi *et al.* (49), was based on molecular modeling. *B,* molecular model of the secondary structure of the α3LG45 domain pair. The three disulfide bonds formed by cysteines 1354–1617, 1507–1530, and 1682–1710 are shown in *yellow*. Residues mutated in this study are depicted in *ball-and-stick* representations: *red* and *blue* indicate residues with and without effects on heparin binding, respectively; *green* indicates residues involved in syndecan-4 interactions. *C,* electrostatic surface potential is represented in the same orientation and on the same scale as in *B,* and negative and positive potentials are shown in *red* and *blue,* respectively. Residues shown in *B* are rendered here in space-filling CPK models, with the same color-coding used in *B*. A probe radius of 1.4 Å was applied.

HS was reported to be of importance (53). We have not investigated whether the specificity observed depends on the GAG compositions or their sulfation levels in this study. Future analysis will be carried out to determine the molecular basis of the glycosaminoglycan interaction specificity. In addition, our data showing binding of the syndecan-4 core protein to the laminin α3LG45 are novel. This interaction is likely to contribute to the syndecan-4-specific interaction. These findings corroborate previous studies showing the involvement of the core protein in syndecan-4 interaction and function (54, 55).

Specific Syndecan-1 and -4 Interactions with α3LG45 May Trigger Specific Cellular Responses—Numerous studies have indicated that the LG45 domain of the human LN332 α3 chain plays an important role in controlling cellular behavior, and it is believed to interact with HSPG cellular receptors, either in an immobilized or soluble manner. In normal conditions, after secretion and deposition in the BM, LN332 rapidly undergoes specific processing, including the cleavage of its LG45 domain. This cleavage allows the first three LG1–3 domains to bind integrins and support biological activities in epithelial BMs (33, 56, 57). Some studies have revealed that the LG45 domain can function both in the full-length LN332 molecule and after it is processed and released. When syndecan-1 was allowed to interact with immobilized LG45 either alone or within pre-LN332, it induced the formation of protrusive adhesion structures through activation of Rac and Cdc42 GTPases (30). Our cell adhesion experiments revealed that Lys-1434, Arg-1436, and Lys-1438 residues are required for syndecan-1-mediated cell adhesion and Arg-1436 or Lys-1438 for protrusion elongation (Fig. 4). We previously showed that syndecan-4 is not involved in this mechanism (30), and we confirmed here that residues specific for the syndecan-4 interaction (Lys-1440/ Lys-1442) were not involved in syndecan-1-mediated cell adhesion. Other *in vitro* studies reported that adding either recombinant α3LG45 or LG4 to the culture medium could induce migration of NHK (26). It was further suggested that this migration depended on a specific sequence within LG4 (^{1412}NSFMALYLSKGR; see Ref. 23). We have confirmed that the WT LG45 domain induces keratinocyte motility, and we have shown that this property is dependent on the syndecan-4 binding domain. These results reinforce previous data that LG45 had a specific syndecan-4-dependent mobilizing effect (27). In contrast to that study attributing the effect to ^{1412}NSFMALYLSKGR based on synthetic peptides, we found that in native α3LG45, this property is carried by residues ^{1436}RIKSKEK.

In this study, we have identified syndecan-1- and -4-binding sites in the α3LG45 domain of LN332. Our results provide the first evidence that specific residues in α3LG45 interact with each of these syndecans. Several lines of evidence have suggested that LG45 is connected to LN332 in the ECM during wound repair (12, 16, 58, 59). LG45 in full-length LN332 was shown to play a central role in the polarization and migration of cells (18, 60) and syndecan-1 binding to LG45 was shown to support keratinocyte migration over immobilized full-length LN332 (29, 30). Moreover, the LG45 region has also been demonstrated to function in the deposition and/or retention of full-length LN332 in the ECM (19, 61, 62). The identification of the syndecan-1- and -4-binding sites in the LN332 LG45 domain is a first step toward understanding of the function of these syndecans in keratinocyte biology.

Acknowledgments—We thank Dr. François Letourneur (Centre de Génétique et de Physiologie Moléculaire et Cellulaire, Lyon, France) for help in designing the mutant constructs and for fruitful discussions. We thank Dr. Neil Smyth (University of Southampton) for providing the expression vector pCEP-Pu. We acknowledge the contribution of the PLATIM platform (Claire Lionnet and Christophe Chamot) of SFR Biosciences Gerland-Lyon Sud (UMS344/US8). We also acknowledge the Partnership for Structural Biology and Institut de Biologie Structurale platforms for access to the Biacore facility (Isabelle Bally and Nicole Thielens).

REFERENCES

1. Alexopoulou, A. N., Multhaupt, H. A., and Couchman, J. R. (2007) Syndecans in wound healing, inflammation, and vascular biology. *Int. J. Biochem. Cell Biol.* **39,** 505–528
2. Morgan, M. R., Humphries, M. J., and Bass, M. D. (2007) Synergistic control of cell adhesion by integrins and syndecans. *Nat. Rev. Mol. Cell Biol.* **8,** 957–969
3. Streuli, C. H., and Akhtar, N. (2009) Signal cooperation between integrins and other receptor systems. *Biochem. J.* **418,** 491–506
4. Zimmermann, P., and David, G. (1999) The syndecans, tuners of transmembrane signaling. *FASEB J.* **13,** S91–S100
5. Couchman, J. R. (2010) Transmembrane signaling proteoglycans. *Annu. Rev. Cell Dev. Biol.* **26,** 89–114
6. Suzuki, N., Nakatsuka, H., Mochizuki, M., Nishi, N., Kadoya, Y., Utani, A., Oishi, S., Fujii, N., Kleinman, H. K., and Nomizu, M. (2003) Biological activities of homologous loop regions in the laminin α chain G domains. *J. Biol. Chem.* **278,** 45697–45705
7. Sasaki, T., Fässler, R., and Hohenester, E. (2004) Laminin. The crux of basement membrane assembly. *J. Cell Biol.* **164,** 959–963
8. Durbeej, M. (2010) Laminins. *Cell Tissue Res.* **339,** 259–268
9. Rousselle, P., Lunstrum, G. P., Keene, D. R., and Burgeson, R. E. (1991) Kalinin. An epithelium-specific basement membrane adhesion molecule that is a component of anchoring filaments. *J. Cell Biol.* **114,** 567–576
10. Rousselle, P., Keene, D. R., Ruggiero, F., Champliaud, M. F., van der Rest, M., and Burgeson, R. E. (1997) Laminin 5 binds the NC-1 domain of type VII collagen. *J. Cell Biol.* **138,** 719–728
11. Aumailley, M., Bruckner-Tuderman, L., Carter, W. G., Deutzmann, R., Edgar, D., Ekblom, P., Engel, J., Engvall, E., Hohenester, E., Jones, J. C., Kleinman, H. K., Marinkovich, M. P., Martin, G. R., Mayer, U., Meneguzzi, G., Miner, J. H., Miyazaki, K., Patarroyo, M., Paulsson, M., Quaranta, V., Sanes, J. R., Sasaki, T., Sekiguchi, K., Sorokin, L. M., Talts, J. F., Tryggvason, K., Uitto, J., Virtanen, I., von der Mark, K., Wewer, U. M., Yamada, Y., and Yurchenco, P. D. (2005) A simplified laminin nomenclature. *Matrix Biol.* **24,** 326–332
12. Lampe, P. D., Nguyen, B. P., Gil, S., Usui, M., Olerud, J., Takada, Y., and Carter, W. G. (1998) Cellular interaction of integrin α3β1 with laminin 5 promotes gap junctional communication. *J. Cell Biol.* **143,** 1735–1747
13. Goldfinger, L. E., Hopkinson, S. B., deHart, G. W., Collawn, S., Couchman, J. R., and Jones, J. C. (1999) The α3 laminin subunit, α6β4 and α3β1 integrin coordinately regulate wound healing in cultured epithelial cells and in the skin. *J. Cell Sci.* **112,** 2615–2629
14. Tunggal, L., Ravaux, J., Pesch, M., Smola, H., Krieg, T., Gaill, F., Sasaki, T., Timpl, R., Mauch, C., and Aumailley, M. (2002) Defective laminin 5 processing in cylindroma cells. *Am. J. Pathol.* **160,** 459–468
15. Ryan, M. C., Lee, K., Miyashita, Y., and Carter, W. G. (1999) Targeted disruption of the *LAMA3* gene in mice reveals abnormalities in survival and late stage differentiation of epithelial cells. *J. Cell Biol.* **145,** 1309–1323
16. Nguyen, B. P., Ryan, M. C., Gil, S. G., and Carter, W. G. (2000) Deposition of laminin 5 in epidermal wounds regulates integrin signaling and adhesion. *Curr. Opin. Cell Biol.* **12,** 554–562
17. Hintermann, E., and Quaranta, V. (2004) Epithelial cell motility on laminin-5. Regulation by matrix assembly, proteolysis, integrins, and erbB receptors. *Matrix Biol.* **23,** 75–85
18. Frank, D. E., and Carter, W. G. (2004) Laminin 5 deposition regulates keratinocyte polarization and persistent migration. *J. Cell Sci.* **117,** 1351–1363
19. Tran, M., Rousselle, P., Nokelainen, P., Tallapragada, S., Nguyen, N. T., Fincher, E. F., and Marinkovich, M. P. (2008) Targeting a tumor-specific laminin domain critical for human carcinogenesis. *Cancer Res.* **68,** 2885–2894
20. Hoffman, M. P., Engbring, J. A., Nielsen, P. K., Vargas, J., Steinberg, Z., Karmand, A. J., Nomizu, M., Yamada, Y., and Kleinman, H. K. (2001) Cell type-specific differences in glycosaminoglycans modulate the biological activity of a heparin-binding peptide (RKRLQVQLSIRT) from the G domain of the laminin α1 chain. *J. Biol. Chem.* **276,** 22077–22085
21. Mizushima, H., Takamura, H., Miyagi, Y., Kikkawa, Y., Yamanaka, N., Yasumitsu, H., Misugi, K., and Miyazaki, K. (1997) Identification of integrin-dependent and -independent cell adhesion domains in COOH-terminal globular region of laminin-5 α3 chain. *Cell Growth Differ.* **8,** 979–987
22. Vivès, R. R., Crublet, E., Andrieu, J. P., Gagnon, J., Rousselle, P., and Lortat-Jacob, H. (2004) A novel strategy for defining critical amino acid residues involved in protein/glycosaminoglycan interactions. *J. Biol. Chem.* **279,** 54327–54333
23. Utani, A., Nomizu, M., Matsuura, H., Kato, K., Kobayashi, T., Takeda, U., Aota, S., Nielsen, P. K., and Shinkai, H. (2001) A unique sequence of the laminin α3 G domain binds to heparin and promotes cell adhesion through syndecan-2 and -4. *J. Biol. Chem.* **276,** 28779–28788
24. Utani, A., Momota, Y., Endo, H., Kasuya, Y., Beck, K., Suzuki, N., Nomizu, M., and Shinkai, H. (2003) Laminin α3 LG4 module induces matrix metalloproteinase-1 through mitogen-activated protein kinase signaling. *J. Biol. Chem.* **278,** 34483–34490
25. Kato, K., Utani, A., Suzuki, N., Mochizuki, M., Yamada, M., Nishi, N., Matsuura, H., Shinkai, H., and Nomizu, M. (2002) Identification of neurite outgrowth promoting sites on the laminin α3 chain G domain. *Biochemistry* **41,** 10747–10753
26. Momota, Y., Suzuki, N., Kasuya, Y., Kobayashi, T., Mizoguchi, M., Yokoyama, F., Nomizu, M., Shinkai, H., Iwasaki, T., and Utani, A. (2005) Laminin α3 LG4 module induces keratinocyte migration. Involvement of matrix metalloproteinase-9. *J. Recept. Signal. Transduct. Res.* **25,** 1–17
27. Araki, E., Momota, Y., Togo, T., Tanioka, M., Hozumi, K., Nomizu, M., Miyachi, Y., and Utani, A. (2009) Clustering of syndecan-4 and integrin β1 by laminin α3 chain-derived peptide promotes keratinocyte migration. *Mol. Biol. Cell* **20,** 3012–3024
28. Décline, F., Okamoto, O., Mallein-Gerin, F., Helbert, B., Bernaud, J., Rigal, D., and Rousselle P. (2003) Keratinocyte motility induced by TGF-β1 is accompanied by dramatic changes in cellular interactions with laminin 5. *Cell Motil. Cytoskeleton* **54,** 64–80
29. Okamoto, O., Bachy, S., Odenthal, U., Bernaud, J., Rigal, D., Lortat-Jacob, H., Smyth, N., and Rousselle, P. (2003) Normal human keratinocytes bind to the α3LG4/5 domain of unprocessed laminin-5 through the receptor syndecan-1. *J. Biol. Chem.* **278,** 44168–44177
30. Bachy, S., Letourneur, F., and Rousselle, P. (2008) Syndecan-1 interaction with the LG4/5 domain in laminin-332 is essential for keratinocyte migration. *J. Cell. Physiol.* **214,** 238–249

31. Sulka, B., Lortat-Jacob, H., Terreux, R., Letourneur, F., and Rousselle, P. (2009) Tyrosine dephosphorylation of the syndecan-1 PDZ binding domain regulates syntenin-1 recruitment. *J. Biol. Chem.* **284,** 10659–10671
32. Kohfeldt, E., Maurer, P., Vannahme, C., and Timpl, R. (1997) Properties of the extracellular calcium binding module of the proteoglycan testican. *FEBS Lett.* **414,** 557–561
33. Rousselle, P., and Aumailley, M. (1994) Kalinin is more efficient than laminin in promoting adhesion of primary keratinocytes and some other epithelial cells and has a different requirement for integrin receptors. *J. Cell Biol.* **125,** 205–214
34. De Hauwer, C., Camby, I., Darro, F., Decaestecker, C., Gras, T., Salmon, I., Kiss, R., and Van Ham P. (1997) Dynamic characterization of glioblastoma cell motility. *Biochem. Biophys. Res. Commun.* **232,** 267–272
35. Pace, C. N., Vajdos, F., Fee, L., Grimsley, G., and Gray, T. (1995) How to measure and predict the molar absorption coefficient of a protein. *Protein Sci.* **11,** 2411–2423
36. Johnson, W. C. (1999) Analyzing protein circular dichroism spectra for accurate secondary structures. *Proteins* **35,** 307–312
37. Whitmore, L., and Wallace, B. A. (2004) DICHROWEB, an on-line server for protein secondary structure analyses from circular dichroism spectroscopic data. *Nucleic Acids Res.* **32,** 668–673
38. Lees, J. G., Miles, A. J., Wien, F., and Wallace, B. A. (2006) A reference database for circular dichroism spectroscopy covering fold and secondary structure space. *Bioinformatics* **22,** 1955–1962
39. Sreerama, N., and Woody, R. W. (2000) Estimation of protein secondary structure from circular dichroism spectra. Comparison on CONTIN, SELCON, and CDSSTR methods with an expanded reference set. *Anal. Biochem.* **28,** 252–260
40. Marky, L. A., and Breslauer, K. J. (1987) Calculating thermodynamic data for transitions of any molecularity from equilibrium melting curves. *Biopolymers* **26,** 1601–1620
41. Sarrazin, S., Bonnaffé, D., Lubineau, A., and Lortat-Jacob, H. (2005) Heparan sulfate mimicry. A synthetic glycoconjugate that recognizes the heparin binding domain of interferon-γ inhibits the cytokine activity. *J. Biol. Chem.* **280,** 37558–37564
42. Arnold, K., Bordoli, L., Kopp, J., and Schwede, T. (2006) The SWISS-MODEL workspace. A web-based environment for protein structure homology modeling. *Bioinformatics* **22,** 195–201
43. Harrison, D., Hussain, S. A., Combs, A. C., Ervasti, J. M., Yurchenco, P. D., and Hohenester, E. (2007) Crystal structure and cell surface anchorage sites of laminin α1LG4-5. *J. Biol. Chem.* **282,** 11573–11581
44. Andac, Z., Sasaki, T., Mann, K., Brancaccio, A., Deutzmann, R., and Timpl, R. (1999) Analysis of heparin, α-dystroglycan, and sulfatide binding to the G domain of the laminin α1 chain by site-directed mutagenesis. *J. Mol. Biol.* **287,** 253–264
45. Wizemann, H., Garbe, J. H., Friedrich, M. V., Timpl, R., Sasaki, T., and Hohenester, E. (2003) Distinct requirements for heparin and α-dystroglycan binding revealed by structure-based mutagenesis of the laminin α2 LG4-LG5 domain pair. *J. Mol. Biol.* **332,** 635–642
46. Yamashita, H., Beck, K., and Kitagawa, Y. (2004) Heparin binds to the laminin α4 chain LG4 domain at a site different from that found for other laminins. *J. Mol. Biol.* **335,** 1145–1149
47. Hoffman, M. P., Nomizu, M., Roque, E., Lee, S., Jung, D. W., Yamada, Y., and Kleinman, H. K. (1998) Laminin-1 and laminin-2 G-domain synthetic peptides bind syndecan-1 and are involved in acinar formation of a human submandibular gland cell line. *J. Biol. Chem.* **273,** 28633–28641
48. Beck, K., Gruber, T. M., Ridgway, C. C., Hughes, W., Sui, L., and Pétra, P. H. (1997) Secondary structure and shape of plasma sex steroid-binding protein. Comparison with domain G of laminin results in a structural model of plasma sex steroid-binding protein. *Eur. J. Biochem.* **247,** 339–347
49. Tisi, D., Talts, J. F., Timpl, R., and Hohenester, E. (2000) Structure of the C-terminal laminin G-like domain pair of the laminin α2 chain harboring binding sites for α-dystroglycan and heparin. *EMBO J.* **19,** 1432–1440
50. Urushibata, S., Katagiri, F., Takaki, S., Yamada, Y., Fujimori, C., Hozumi, K., Kikkawa, Y., Kadoya, Y., and Nomizu, M. (2009) Biologically active sequences in the mouse laminin α3 chain G domain. *Biochemistry* **48,** 10522–10532
51. Talts, J. F., Andac, Z., Göhring, W., Brancaccio, A., and Timpl, R. (1999) Binding of the G domains of laminin α1 and α2 chains and perlecan to heparin, sulfatides, α-dystroglycan, and several extracellular matrix proteins. *EMBO J.* **18,** 863–870
52. Hozumi, K., Suzuki, N., Uchiyama, Y., Katagiri, F., Kikkawa, Y., and Nomizu, M. (2009) Chain-specific heparin-binding sequences in the laminin α chain LG45 modules. *Biochemistry* **48,** 5375–5381
53. Kreuger, J., Spillmann, D., Li, J. P., and Lindahl, U. (2006) Interactions between heparan sulfate and proteins. The concept of specificity. *J. Cell Biol.* **174,** 323–327
54. Rapraeger, A. C., and Ott, V. L. (1998) Molecular interactions of the syndecan core proteins. *Curr. Opin. Cell Biol.* **10,** 620–628
55. Echtermeyer, F., Baciu, P. C., Saoncella, S., Ge, Y., and Goetinck, P. F. (1999) Syndecan-4 core protein is sufficient for the assembly of focal adhesions and actin stress fibers. *J. Cell Sci.* **112,** 3433–3441
56. Carter, W. G., Ryan, M. C., and Gahr, P. J. (1991) Epiligrin, a new cell adhesion ligand for integrin α3β1 in epithelial basement membranes. *Cell* **65,** 599–610
57. Sonnenberg, A., de Melker, A. A., Martinez de Velasco, A. M., Janssen, H., Calafat, J., and Niessen, C. M. (1993) Formation of hemidesmosomes in cells of a transformed murine mammary tumor cell line and mechanisms involved in adherence of these cells to laminin and kalinin. *J. Cell Sci.* **106,** 1083–1102
58. Ryan, M. C., Tizard, R., VanDevanter, D. R., and Carter, W. G. (1994) Cloning of the *LamA3* gene encoding the α3 chain of the adhesive ligand epiligrin. Expression in wound repair. *J. Biol. Chem.* **269,** 22779–22787
59. Decline, F., and Rousselle, P. (2001) Keratinocyte migration requires α2β1 integrin-mediated interaction with the laminin 5 γ2 chain. *J. Cell Sci.* **114,** 811–823
60. Goldfinger, L. E., Stack, M. S., and Jones, J. C. (1998) Processing of laminin-5 and its functional consequences. Role of plasmin and tissue-type plasminogen activator. *J. Cell Biol.* **141,** 255–265
61. Sigle, R. O., Gil, S. G., Bhattacharya, M., Ryan, M. C., Yang, T. M., Brown, T. A., Boutaud, A., Miyashita, Y., Olerud, J., and Carter, W. G. (2004) Globular domains 4/5 of the laminin α3 chain mediate deposition of precursor laminin 5. *J. Cell Sci.* **117,** 4481–4494
62. Tsubota, Y., Yasuda, C., Kariya, Y., Ogawa, T., Hirosaki, T., Mizushima, H., and Miyazaki, K. (2005) Regulation of biological activity and matrix assembly of laminin-5 by COOH-terminal LG4–5 domain of α3 chain. *J. Biol. Chem.* **280,** 14370–14377

Cell Surface Proteoglycans Syndecan-1 and -4 Bind Overlapping but Distinct Sites in Laminin α3 LG45 Protein Domain

Sonia Carulli, Konrad Beck, Guila Dayan, Sophie Boulesteix, Hugues Lortat-Jacob and Patricia Rousselle

J. Biol. Chem. 2012, 287:12204-12216.
doi: 10.1074/jbc.M111.300061 originally published online February 20, 2012
